Estuaries and Coasts
https://doi.org/10.1007/s12237-022-01098-2

Kelp Forest Drag Coefficients Derived from Tidal Flow Data

Stephen Monismith[1] · Maha Alnajjar[1] · Margaret Daly[1] · Arnoldo Valle-Levinson[2] · Braulio Juarez[3] · Matheus Fagundes[4] · Tom Bell[5] · C. Brock Woodson[4]

Received: 10 December 2021 / Revised: 5 May 2022 / Accepted: 3 June 2022

Abstract

We present an approach for estimating drag coefficients for depth-averaged tidal flows that uses the ratio of observed RMS velocities to the RMS velocities that would be observed without bottom friction. We find that this ratio, R, depends on a single non-dimensional number, $P = C_D C\eta_0/\omega H^2$, where C_D is the drag coefficient, and C is the phase speed of a tidal wave with amplitude η_0 and frequency ω, in water of depth h. The function $R(P)$ can be inverted to solve for C_D using measured values of R. Taking advantage of a unique multi-year record of tidal flows on Isla Nativdad, Baja California, Mexico, during which time the kelp forest there varied between non-existent and dense, we use this method to quantify the effect of kelp biomass on drag. This analysis shows that a maximum value of $C_D \approx 0.04$ is reached for relatively low values of kelp biomass, which may be an effect of sheltering (reductions in the velocity creating drag due to the close proximity of bundles of kelp stipes). However, values as large as 0.015 were observed when the water column experienced strong secondary flows in the presence of strong density stratification. Given that the long-term measurements were made near a coastal headland, we argue that this may reflect variations in secondary flow strength due to stratification. Lastly, our measurements show little evidence of enhancement of drag by surface waves.

Introduction

Nearshore coastal flows over coral reefs or through kelp forests are typically affected by frictional drag. Conventionally, drag associated with bottom friction is computed using a drag coefficient, C_D, defined in terms of the bottom stress, $\vec{\tau}_b$, and a reference velocity $\vec{U}_r$:

$$\vec{\tau}_b = \rho C_D \overline{U}_r \| \overline{U}_r \| \tag{1}$$

where ρ is water density. The reference velocity in shallow flows is the depth-averaged velocity (Lentz et al. 2017), whereas in many cases it is the velocity measured 1 m above the bed (Reidenbach et al. 2006). For the latter case on relatively smooth surfaces (e.g., the muddy bottom of an estuary), $C_D \approx 0.003$, whereas for coral reefs C_D is generally one order of magnitude larger (Reidenbach et al. 2006). Values of C_D based on depth-averaged velocities depend on overall depth, bottom roughness (Lentz et al. 2017; Rogers et al. 2018), the presence of waves (Grant and Madsen 1979; Lentz et al. 2018), and, for flexible roughness elements (e.g., seagrasses or macroalgae), flow speed (Nepf 2012). However, in the case of canopy flows like those over coral reefs or submerged seagrass beds or flows with fully emergent vegetation, what is referred to as bottom stress is the area- and depth-averaged effect of the drag forces exerted on the flow by the various roughness elements (Rosman and Hench 2011).

One form of living roughness commonly found in the nearshore of upwelling regions like California is the large kelp *Macrocystis pyrifera*, which has been observed to reduce flow speed (Jackson and Winant 1983; Gaylord et al. 2007;

Communicated by David K. Ralston

✉ Stephen Monismith
monismith@stanford.edu

1 Department of Civil and Environmental Engineering, Stanford University, Stanford, CA 94305-4020, USA

2 Department of Civil & Coastal Engineering, University of Florida, Gainesville, FL 32603, USA

3 Instituto de Investigaciones Oceanológicas, Universidad Autonoma de Baja California, Ensenada, Mexico

4 College of Engineering, University of Georgia, Athens, GA 30602, USA

5 Department of Applied Ocean Physics & Engineering, Woods Hole Oceanographic Institution, Woods Hole, MA 02543, USA

Published online: 14 July 2022

Rosman et al. 2007), presumably because the plants extend throughout the water column and exert an increased drag force. As discussed in Rosman et al. (2010, 2013), the physics of drag caused by *Macrocystis pyrifera* is especially complicated because kelp plants can (a) move and deform in response to flow, thus reducing their drag in some cases (Utter and Denny 1996; Gaylord et al. 2003, 2008); (b) have drag elements in the water column (the fronds); (c) have a floating surface canopy (Rosman et al. 2013); and (d) have interannual variability in growth and density. The physical response of kelp is also different for mean currents and surface waves. In mean currents, kelp is essentially fixed in place relative to flows so that bending is the only response (Gaylord et al. 2003). For surface waves, the kelp plants move in some fashion with the waves (Mullarney and Pilditch 2017), although this relative motion must vary with depth since the kelp stipes are fixed to the benthos by their holdfasts.

Given the complexity of the kelp-flow interaction, it is clearly important to include kelp-drag in circulation models to accurately represent flows in the nearshore coastal ocean. This could be done simply by imposing a depth-averaged body force that per unit volume takes the form (Jackson and Winant 1983):

$$F = \rho C_D^K \frac{A_f}{hB^2} U|U| = \frac{\rho C_D U|U|}{h}, \quad C_D = C_D^K \frac{A_f}{B^2} \tag{2}$$

where C_D^K is the O(1) drag coefficient for flow around kelp plants (fronds, stipes, etc.) that have a frontal area A_f, and are spaced B apart. For rigid objects in the presence of waves and mean currents, the velocity U appearing in Eq. (2) could be taken as the instantaneous velocity, and wave (time)-averaged forces then computed by wave averaging Eq. (2). However, for kelp, the situation is more complex; without knowing the motion of the kelp plants, U, which is in this case the velocity relative to the moving kelp (Rosman and Hench 2011; Gaylord et al. 2003), is effectively unknown.

In this paper, we describe an approach for empirically estimating an effective value of C_D given measurements of velocities and knowledge of the tidally varying sea surface slope. The analysis we present in §3 is developed to estimate kelp-biomass-dependent effective drag coefficients for depth-averaged flows through the kelp (*M. pyrifera*) forests found in the nearshore of Isla Natividad, Baja California Sur, Mexico. These kelp forests have been the focus of long-term studies of biophysical interactions in support of management of various fisheries that include the red abalone (Boch et al. 2017, 2018; Woodson et al. 2018; Al Najjar 2019).

The Observational Data Set

As part of our studies of the Natividad kelp forests, multi-year deployments of 1 MHz Nortek acoustic Doppler profilers were made in ca. 15 m of water on both sides (east and west) of Isla Natividad, Baja California (Alnajjar 2019; Monismith et al. unpublished; Fig. 1). One site, Morro Prieto, on the west side, experiences both upwelling and tidal flows, whereas Punta Prieta on the east is strongly tidal. At both sites, the ADP were in small clearings in the kelp forest and were configured to take profiles every 5 to 20 min (several different intervals were used) with a vertical resolution of 0.5 m. for 3 to 6 months (the time between deployments and recoveries also varied). Along with the ADP, there was also a bottom mounted Seabird SBE37 CTD and a mooring with Seabird SBE 56 thermistors at 1, 6, and 11 mab. The first series of measurements were made between April 2013 and October 2015, and a second set of deployments at both sites was made between August 2018 and Sept. 2019. This second deployment followed the same design as the 2013–2015 deployments. Sampling parameters for the various deployments are shown in Table 1 (adapted from Monismith et al. unpublished). The singular feature of this unique data set is that these measurements include a period of anomalously high temperatures in the Eastern Pacific, a period generally referred to as "The Warm Blob" (Cavole et al. 2016; Di Lorenzo and Mantua 2016), that led to the complete disappearance of kelp from Isla Natividad (Alnajjar 2019). In addition to mean velocity profiles, in 4 of the first set of deployments, wave burst data were recorded for near-bottom wave velocities. Examination of these wave data shows a remarkable degree of agreement between what would be predicted from linear wave theory using the measured variations in pressure and measured wave velocities (Monismith et al. unpublished). Where required, Godin filtering (Godin 1972) was used to compute RMS (root mean square) values of various quantities such as depth-averaged tidal currents.

To quantify the effect of kelp biomass on drag, we used satellite-based computed from Landsat data (Bell et al. 2018). These estimates are made for 30×30-m tiles, albeit at somewhat variable intervals of time, given cloud cover, and other factors that can obscure the site. Satellite-derived kelp biomass estimates mostly reflect the surface canopy, although the in-water biomass, e.g., stipes and blades, is monotonically related to canopy biomass.

In what follows, we develop a simple theory for using measurements of tidal currents and free surface variations to estimate C_D. We then use the Punta Prieta (east side) current

Table 1 Instruments and sampling details (adapted from Monismith et al. unpublished)

Dates	**Mean velocity**: Sample interval Averaging period Bin size	**Wave sampling**: Sample interval No. samples (@1 Hz) Wave bin size	**Thermistor chain:** Sample interval Heights
3/7/13 to 7/2/13	10 min 1 min 0.5 m bins	none	Variable – averaged to 0.5 h 1, 6, 11 mab
7/4/13 to 9/9/13	10 min 1 min 0.5 m	1 h 1024 1 m	Variable – averaged to 0.5 h 1, 6, 11 mab
9/13/13 to 3/29/14	5 min 30 s 0.5 m	1 h 1024 2 m	Variable – averaged to 0.5 h 1, 6, 11 mab
3/31/14 to 2/20/15	10 min 1 min 0.5 m	1 h 1024 2 m	Variable – averaged to 0.5 h 1, 6, 11 mab
3/16/15 to 9/11/15	30 min 1 min 0.5 m	none	Variable – averaged to 0.5 h 1, 6, 11 mab
8/16/18 to 8/11/19	10 min 20 s 1 m	1 h 1024 2 m	Variable – averaged to 0.5 h 1, 6, 11 mab

data to estimate drag, since the relevant pressure gradients there are primarily tidal, and thus amenable to estimation, whereas for Morro Prieto (west side), both tides and larger-scale wind-driven flows matter, a situation for which pressure gradients are difficult to estimate a priori.

A Simple Model of The Dynamics of Frictional Tidal Currents

Theory

A simple model of the effect of kelp on tidal current strength can be constructed using the 1D, linear momentum equation for a homogeneous, depth-averaged alongshore flow driven by a tidally varying barotropic pressure gradient (Arzeno et al. 2018):

$$\frac{\partial U}{\partial t} + C_D \frac{U|U|}{h} = -g\frac{\partial \eta}{\partial x} \tag{3}$$

here, h is the depth, U is the depth-averaged alongshore (x direction) velocity, and η is the free surface deflection.

If the tide can be modeled as a progressive wave propagating at speed C (which is not necessarily determined by the local depth):

$$\frac{\partial \eta}{\partial x} = -\frac{1}{C}\frac{\partial \eta}{\partial t} = -\frac{1}{\sqrt{gh}}\frac{\partial \eta}{\partial t}. \tag{4}$$

Thus:

$$\frac{\partial U}{\partial t} + C_D \frac{U|U|}{h} = \frac{C}{h}\frac{\partial \eta}{\partial t}. \tag{5}$$

In the absence of drag, it can be shown that:

$$U_{rms} = \frac{C}{h}\eta_{rms} = U^I_{rms}, \tag{6}$$

where U^I_{rms} is the rms inviscid velocity. Thus, the ratio $R = U_{rms}/U^I_{rms}$ is a measure of the importance of drag. Values of R range between 0 and 1, with 1 being inviscid flow. A plot of the dependence of this ratio for $h = 15$ m as functions of C_D and η_{rms} is shown in Fig. 2. Notably, the inclusion of quadratic drag causes U_{rms}/U^I_{rms} to decline as η_{rms} increases, meaning that U_{rms}/U^I_{rms} will be smaller (i.e., more frictional flow) at spring tides than at neaps.

For a single tidal constituent, Eq. (5) can be scaled using the inviscid solution to produce the non-dimensional variables denoted by *:

$$U = \left(C\eta_0/h\right)U^* \quad t = \omega^{-1}t^* \quad \eta = \eta_0\eta^* \tag{7}$$

where ω is the tidal frequency and η_0 is the RMS tidal amplitude. Using this scaling, the non-dimensional x momentum equation becomes:

$$\frac{\partial U^*}{\partial t^*} + PU^*|U^*| = \frac{\partial \eta^*}{\partial t^*} \tag{8}$$

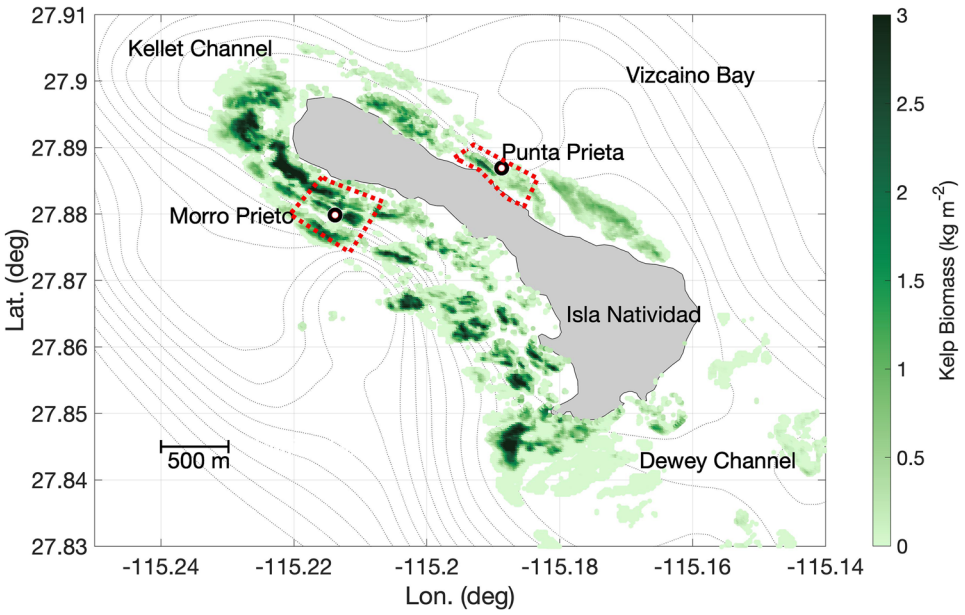

Fig. 1 Isla Natividad: the locations of the two long-term deployments are shown as are average values of kelp biomass for the period April 2013 to October 2015 (taken from Monismith et al. unpublished, used by permission). The dashed red boxes denote the areas used to estimate values of kelp biomass density that might influence currents at the ADP sites

where the parameter determining the importance of drag is:

$$P = \frac{C_D C \eta_0}{\omega h^2} \tag{9}$$

Note that R equals the rms value of U^* calculated by solving Eq. (8). Per the Buckingham Pi theorem (e.g., Street et al. 1996), as we have defined the problem, there are 6 parameters, U_{rms}, C_D, C, η_0, ω, and h, having 2 dimensions (length and time). Thus, there are 4 possible dimensionless parameters, two of which are R and P. A third is η_0/h which could be important if h in the denominator of Eq. (3) was replaced with $\eta_0 f(t) + h$. The 4th parameter could be $C/\sqrt{gh}$. However, evidently if both C and h are specified separately as we do below, this 4th parameter does not explicitly influence the determination of U^* and thus R.

The function $R(P)$ found by numerical integration is shown in Fig. 3, where it can be seen that for $P \to 0, R \to 1$ and that $P \to 1, R \to 0$. P is similar to the non-dimensional parameter Prandle and Rahman (1980) used to examine effects of convergence and friction on tidal propagation in

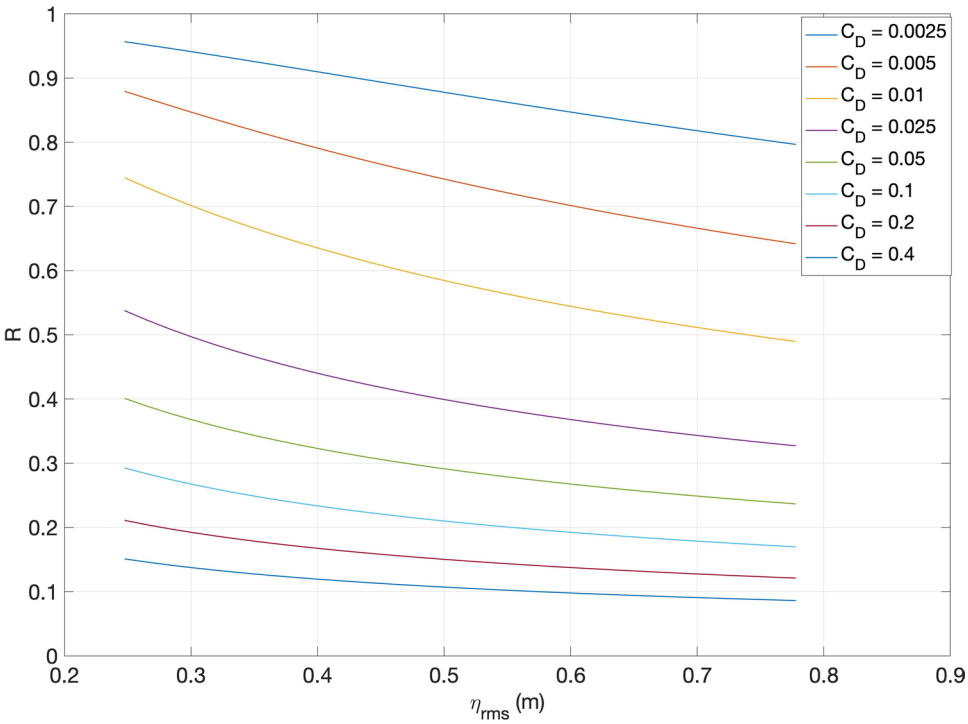

Fig. 2 Ratio of computed RMS depth-averaged velocity to its value on the absence of drag for an M2 tide for $h = 15$ m of water, with $C = \sqrt{gh}$, and various values of C_D

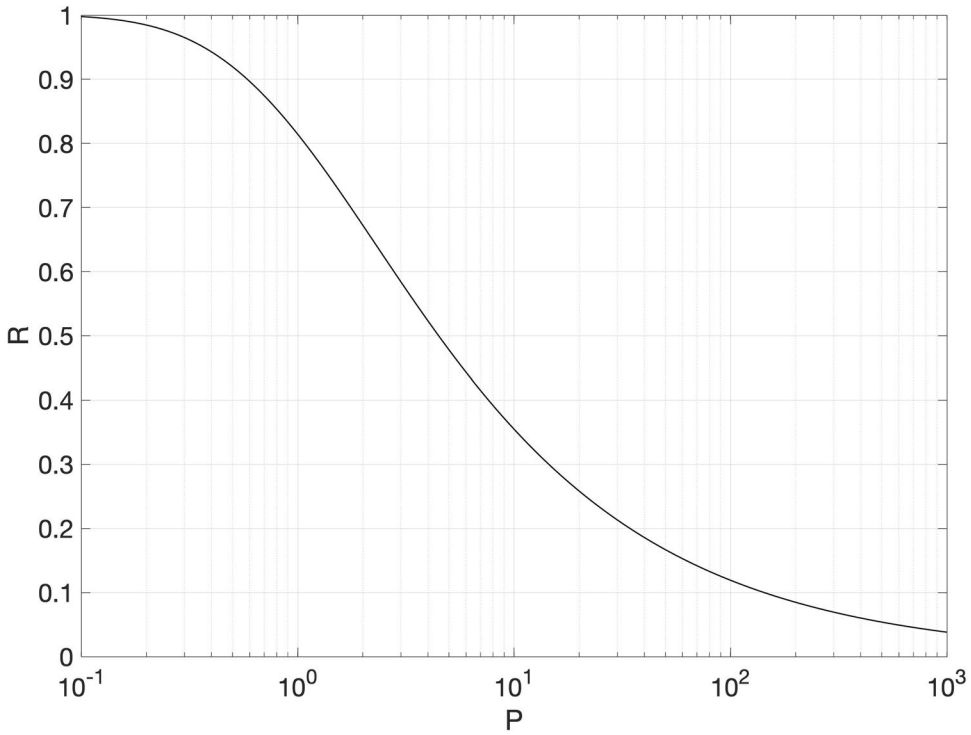

Fig. 3 RMS velocity ratio R as a function of the drag parameter P

estuaries. The difference is that Prandle and Rahman used linearized bottom friction whereas Eq. (9) is based on quadratic drag.

While solutions to Eq. (8) describe the basic behavior, using this approach for real tidal currents may be more complicated because real tides have multiple constituents and so the effects of drag will vary in time because of phasing of the various constituents. However, Eq. (8) can be numerically integrated using time series data for $\partial\eta/\partial t$ as the forcing. Figure 4 shows this calculation made using water

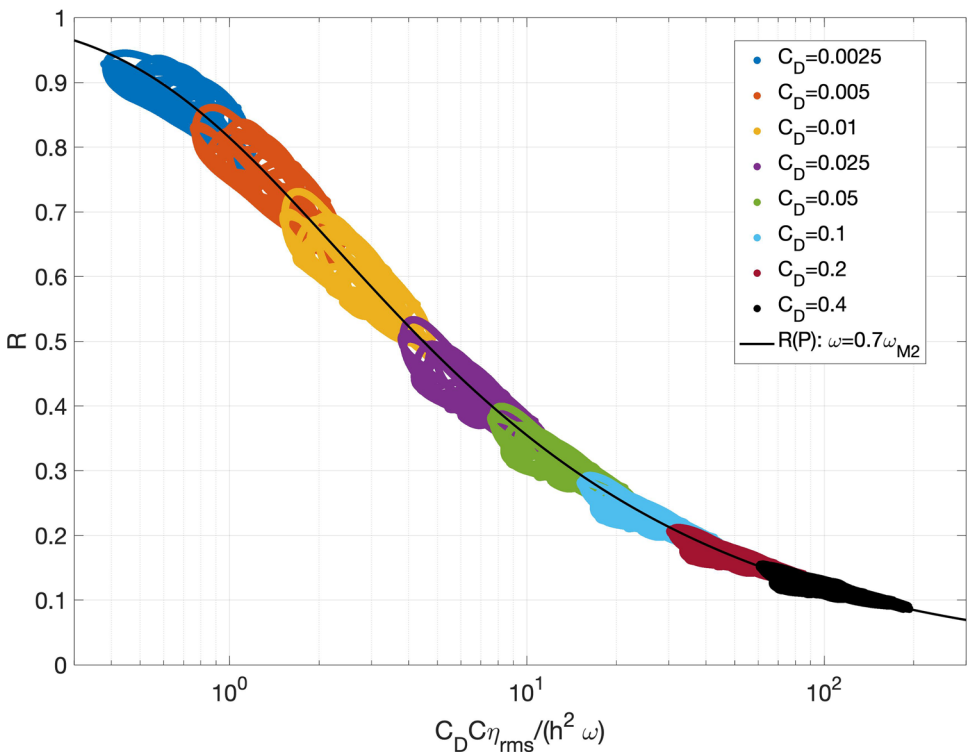

Fig. 4 Scaled RMS velocity ratio R as a function of $P = \left(C_D C\eta_{rms}\right)/\left(h^2\omega\right)$ P computed using time series of free surface elevation from Punta Prieta, Baja California. As shown in the legend, different colored symbols correspond to different values of the C_D, with the lowest value of C_D giving the highest values of R and the lowest value of C_D giving the lowest values of R_s

level data taken at Punta Prieta (east side) between August 2018 and March 2019 and a variety of values of C_D between 0.0025 (a sandy bottom) and the very large value of 0.5. Here, P is defined using an effective value of $\omega = 0.7\omega_{M2}$ where ω_{M2} is the frequency of the M2 tidal constituent (Fig. 4), chosen by trial and error to match the dependence of R on P seen with a single constituent. As seen in Fig. 4, the single constituent model is remarkably effective at collapsing the computed velocities for the more complex case of multiple constituents. It seems likely that the factor of 0.7 found for the Punta Prieta data would not be the same for other locations with different mixes of constituent amplitudes and phases.

Caveats

It should be noted that as with any analysis based on the mean momentum balance, the approach we present here implicitly includes the effects of surface gravity waves (c.f. Lentz et al. 2018). Thus, the values of C_D derived using the approach given above should depend on the strength of whatever surface waves may be present relative to the tidal currents. In effect, if the drag coefficient that might exists in the absence of waves is C_D^0, then, in the presence of waves characterized by velocity U_w, one might expect that $C_D = C_D^0 f\left(U_w/U_{rms}^I\right)$. In effect, if C_D^0 were specified, or was to be determined from observations, then the ratio R would depend on two non-dimensional parameters: (1) P now defined with C_D^0 and (2) the velocity ratio U_w/U_{rms}^I. In principle, this means that values of C_D determined at a given site by inverting the $R(P)$ relationship using observations should depend on wave conditions. While this certainly is true for fixed roughness elements like corals, it may not be the case if the roughness elements, e.g., kelp plants, move with the waves.

Secondly, to the extent the assumptions underlying Eq. (3) are violated, C_D computed using Eq. (3) may differ from the "actual" value of C_D. For example, as written, Eq. (3) neglects advective accelerations; as we discuss below (§4.2), it appears that at times, lateral momentum advection can also increase apparent drag on the longshore flow. The possible effects of stratification are more difficult to predict: For bottom roughness like that of corals, bottom stress is determined by the near-bottom velocity and so, in the presence of stratification, may depend on the depth-averaged flow in a way that varies with stratification strength and structure. For kelp, the drag-causing structures, e.g., stipes and blades, are distributed throughout the water column rather than being located on the bottom, and so, both the distributions of currents and drag elements should matter. Thus, strictly speaking, Eq. (3) can be viewed as best defining C_D when the flow is in fact 1D and unstratified, although it should provide a decent approximation to an appropriate value of C_D to use with depth-averaged flows in many cases.

Lastly, the assumption of progressive wave behavior by the tide may limit the applicability of our approach. Our method appears appropriate for the east side of Isla Natividad, where the tidal motions of interest have a cross-shore length scale that is much larger than the width of the kelp forest (ca. 250 m) because they are associated with the entirety of Vizcaino Bay which is O(100 km) in length and width. In this case, as in classical boundary layer analysis, the pressure gradient inside the (narrow) kelp forest is the same as the pressure gradient outside which is determined by the progressive wave behavior of the tide in Vizcaino Bay. In any case, it seems likely that the theory we present above could be modified to account for phasing appropriate to standing waves, or for the phasing produced by a mixture of standing and progressive waves.

Application of the Theory to Punta Prieta Tidal Currents

Inferring Kelp Biomass Drag Coefficients

The relation between R and P can be used to estimate drag coefficients from measurements if C is known and if the tidal motion is largely progressive, i.e., the observed value of R can be used to find P and then one can solve for C_D using Eq. (8). Here, the goal is to use that information to infer a relationship between kelp biomass and drag. Average estimated biomass for March 2013 to Sept 2015 for 30×30 m pixels at Isla Natividad shows the typical spatial heterogeneity of kelp forests (Fig. 1). This points to a challenge in estimating kelp forest drag: What spatial scale determines the drag at a given location? In the absence of a definitive answer to this question, we assumed that an appropriate averaging spatial scale would be the average tidal excursion. This was used to define the region at Punta Prieta shown in Fig. 1.

Figure 5 shows approximately 3 ½ years of water level, kelp biomass (based on the box shown in Fig. 1), and current data taken at Punta Prieta during two periods: March 2013 to September 2015 and August 2018 to September 2019. During this time, spring-neap tidal variations resulted in values of η_{rms} between 0.3 and 0.8 m, while kelp biomass, and hence drag by kelp, varied by at least one order of magnitude. Reflecting kelp-induced variations in C_D, R ranged from 0.1 to 0.65. The inferred values of C_D depend on C. The value of C here (60 m/s) was chosen so that C_D matched the value (0.005) estimated via fitting velocity profiles to the law of the wall for the period in 2015 when there was no kelp. This value is larger than what is typically seen for flat, sandy beds; it probably reflects the small-scale relief of the rocky substrate that typifies abalone habitat at Isla

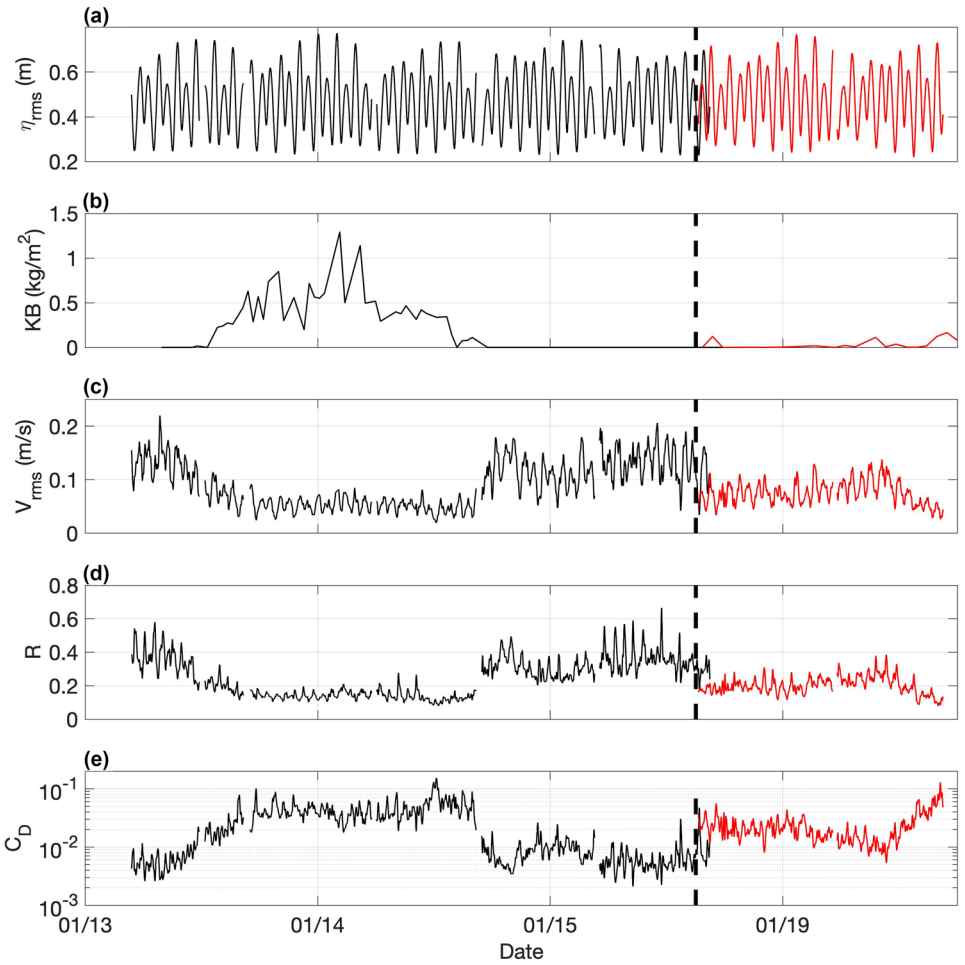

Fig. 5 Conditions at Punta Prieta, Baja Mexico: (**a**) RMS tidal elevation; (**b**) kelp biomass (solid line is for Punta Prieta and the dashed line is an estimate for Punta Prieta based on Morro Prieto (for comparison); (**c**) measured RMS alongshore velocity; (**d**) the RMS velocity ratio R; and (**e**) inferred drag coefficient based on $P(R)$ and an assumed value of $C = 60$ m/s. To the left of the dashed line, the data are from 2013 to 2015 whereas to the right (red lines), the data are from 2018 to 2019

Natividad. Values of C could also be derived from a full tidal circulation model for the region. In any case, using this approach, estimated values of C_D varied between 0.005 and (very rarely) 0.15, the latter close to the value estimated by Jackson and Winant (1983) for the Pt. Loma kelp forest.

Histograms of C_D (Fig. 6) show a minimum of three separate kelp forest states: a no kelp state (2013–2015 data; $C_D = 0.005$ represented by the vertical dashed line of Fig. 6), an intermediate kelp biomass state (2018–2019 data; $C_D \approx 0.02$, red line), and a high kelp biomass state (2013–2015 data; $C_D \approx 0.04$, black line), although the 2013–2015 data do suggest that period of values of C_D has high as 0.06 or more. In light of this, it is not clear whether or not the highest inferred values of C_D, i.e., values greater than 0.1, are physical or are a result of the fact that when R is small, small changes in R will produce large changes in P and hence large changes in C_D. This will be discussed further below.

Combining the kelp biomass estimates (KB) and C_D estimates, one can derive a relationship between the two. This is shown in Fig. 8, where the admittedly scattered data is fit using robust least-squares nonlinear regression (as implemented in MATLAB's curve fitting tool) to the function

$$C_D = a \tanh(bKB) + 0.005$$

where $a = 0.033 \pm 0.003$ and $b = 17 \pm 11$ were found by fitting. The function tanh was chosen because it is the simplest function that describes a smooth transition from one value (0.005) to another (0.04). The fit shown in Fig. 7 to the combined data set (2013–2015 and 2018–2019) has a value of $r^2 = 0.25$. The plateau in $C_D \approx 0.04$ reached for biomass values greater than 0.2 kg/m^2 suggests that the effects of sheltering, i.e., the interaction of wakes of canopy elements (primarily bundles of kelp stipes) that reduces drag inside the canopy (Nepf 2012), become important for relatively small values of kelp biomass.

Effects of Stratification, Secondary Flows, and Surface Waves

However, inferred values of C_D shown in Fig. 5 can at times be considerably larger than the averaged behavior shown in

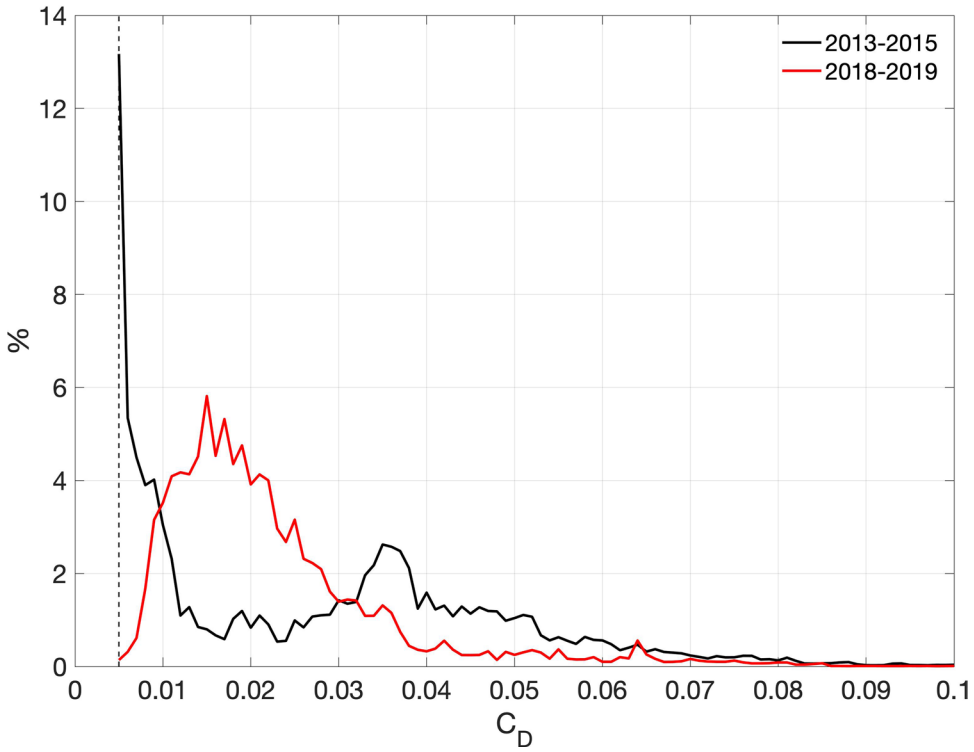

Fig. 6 Histograms of C_D estimated by inverting the function $R(P)$ shown in Fig. 3 and using observed values of R. Separate histograms are shown for the 2013–2015 and 2018–2019 data sets. The dashed line shows the limiting value of C_D (0.005) found for flows at the field site in the absence of kelp

Fig. 7, reaching a value as high as 0.15, comparable to what Jackson and Winant (1983) estimated for flows through the Point Loma kelp forest near San Diego, CA. In the present case, it is useful to examine conditions existing at times when these high values appear. As seen in Fig. 8, values of C_D that are notably larger than values estimated using

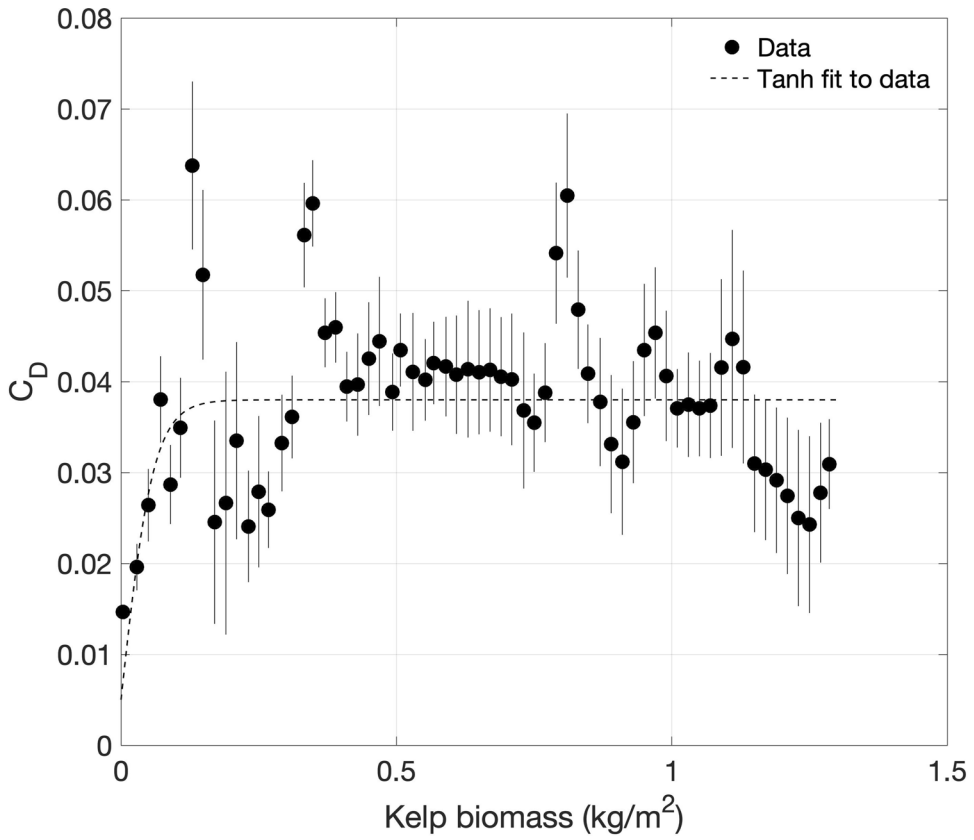

Fig. 7 C_D as a function of kelp biomass at Punta Prieta. Time varying values of C_D have been bin-averaged according to estimated kelp biomass (KB) at each time. The fitted curve ($r^2 = 0.25$) is $C_D = (0.033 \pm 0.003)\tanh[(17 \pm 11)KB] + 0.005$. Error bars associated with variability in bin-averaged data are also included in this plot

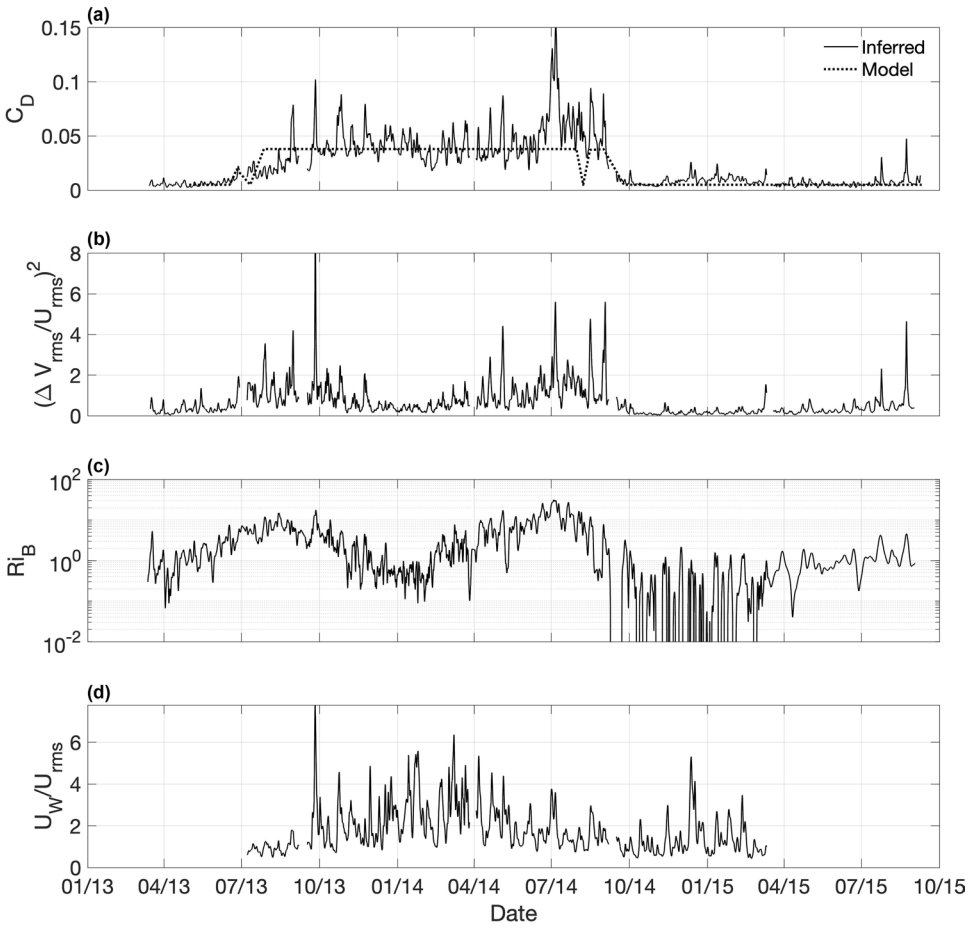

Fig. 8 Conditions in the Punta Prieta kelp forest as observed between March 2013 and September 2015: (**a**) time variability of C_D estimated using the momentum balance (-) and modeled using kelp biomass estimates (⋯); (**b**) strength of cross-shore flow, $(V_{rms}/U_{rms})^2$; (**c**) flow stability as calculated by Eq. (10); (**d**) strength of wave forcing (U_W/U_{rms})

the C_D-KB relation shown in Fig. 7 tend to occur when secondary flows, represented by the RMS strength of the vertical shear in the cross-shore direction, ΔV_{rms}, are relatively strong (Fig. 8b) and when the water column is stable (Fig. 8c), i.e., when the bulk Richardson number is greater than O(1). ΔV_{rms} was calculated as the RMS value of the difference between the near surface ($z = 10.15$ to 11.65 mab) and near-bottom ($z = 0.65$ to 2.15 mab) cross-shore velocities. In Eq. (10), α is the thermal expansivity and ΔT is the measured temperature difference between the bottom and the water surface. In Fig. 8c, Ri_B has been calculated using Godin-filtered values of values of ΔT.

$$Ri_B = -\frac{g\alpha\Delta Th}{U_{rms}^2} \tag{10}$$

While C_D covaries with $\Delta V_{rms}/U_{rms}$ and Ri_B, counter to what might be commonly expected, the strength of surface gravity waves as measured by the ratio of wave RMS velocity, U_W, to U_{rms}, has little discernable influence on inferred values of C_D. As suggested previously (e.g., Gaylord et al. 2003, 2012), this may reflect the fact that the kelp plants move with the waves so as to reduce the drag they experience.

Determining how either stratification or secondary flows or some combination of both is complicated by the fact that the large values of C_D are associated with small values of U_{rms} which also tend to produce the highest values of Ri_B. For example, disregarding any direct effect of secondary flows, i.e., by considering C_D to depend on Ri_B (but not explicitly on $\Delta V_{rms}/U_{rms}$) as well as kelp biomass, one finds a strong relationship between C_D and Ri_B (not shown) such that for $Ri_B > O(1)$, the inferred values of C_D increase with Ri_B, behavior that is quite different from what is commonly seen in estuarine and coastal flows where increasing Ri_B tends to decrease the value of C_D based on depth-averaged flows (e.g., Stacey et al. 1999).

The secondary flows at the Punta Prieta mooring arguably are due to the presence of the headland at Punta Prieta (Valle-Levinson et al. 2022), which introduces streamline curvature into the alongshore flow. The lateral flow at this site should be shoreward at the bottom bringing in higher momentum fluid from offshore and offshore at the surface transporting lower momentum fluid from closer to the shore. A simple model of the effects of secondary flows on the mean alongshore momentum balance can be had by

considering a modified version of Eq. (2) that includes the depth integrated effects of a secondary, cross-shore flow v acting on the lateral shear created by the presence of the kelp:

$$\frac{\partial U}{\partial t} + C_D \frac{U|U|}{h} + \frac{1}{h}\int_0^h v\frac{\partial u}{\partial y}dz = -g\frac{\partial \eta}{\partial x} \tag{11}$$

here, y represents the cross-shore coordinate in a local, mildly curvilinear coordinate system for which $U(y)$ is the depth-averaged alongshore velocity which varies with y, z is the vertical coordinate directed upwards from the bottom, and the local cross-shore (v) and alongshore (u) velocities both vary with y and z. Suppose that:

$$v = \Delta V(y) f_1(z/h) \text{ and } \quad u = \frac{u_*(y)}{\kappa}\log\left(z/z_0\right), \tag{12}$$

where $u_*(y)$ is the shear velocity and z_0 is the bottom roughness. Then:

$$\frac{1}{h}\int_0^h v\frac{\partial u}{\partial y}dz = \frac{\Delta V}{\kappa}\frac{\partial u_*}{\partial y}\left[\frac{1}{h}\int_0^h f_1(z/h)\log\left(z/z_0\right)dz\right] \tag{13}$$

Using the theory of Kalkwijk and Booij (1986) who show that curvature (which radius R_c) creates an approximately linearly sheared secondary flow (assuming a constant bottom drag coefficient $C_D^B = 0.005$) with:

$$\Delta V \approx 2\frac{Uh}{\kappa^2 R_c} \tag{14}$$

The integral term in brackets in Eq. (13) is approximately 3.7 (and only weakly depends on z_0) so that:

$$\begin{aligned}\frac{1}{h}\int_0^h v\frac{\partial u}{\partial y}dz &\approx 7.4\frac{Uh}{\kappa^2 R_c}\frac{\partial u_*}{\partial y} = 7.4\frac{Uh}{\kappa^2 R_c}\frac{\partial}{\partial y}\left(C_D^B U\right)\\ &= 7.4 C_D^B \frac{U^2(y_m)h}{\kappa^2 R_c Y}\end{aligned} \tag{15}$$

where (1) U (y_m) is the velocity at the location, $y = y_m$, at which we have made measurements; (2) we have assumed that C_D^B is constant; and (3) Y is a length scale such that $\partial U/\partial y \equiv U/Y$. Thus, there is an extra drag term that has the same sign as the effective drag associated with the kelp and bottom, and so the large values of C_D may reflect the effects of secondary flows.

While this argument is consistent with our data, it appears to have a shortcoming: Eq. (14) predicts that the ratio $\Delta V/U$ (plotted as $\Delta V_{rms}/U_{rms}$) should be constant. Instead, it is observed to vary considerably (Fig. 8b). However, this variation appears to be connected to stratification. While for values of $Ri_B < 0.3$, $\Delta V_{rms}/U_{rms} \approx 0.4$, $\Delta V_{rms}/U_{rm}$ increases with Ri_B for $Ri_B > 0.3$, such that for $Ri_B \approx 10$, $\Delta V_{rms}/U_{rms} \approx 1.3$ (Fig. 9). This behavior, stronger secondary flows in the presence of stratification, has been observed in estuarine flows as well (Nidzieko et al. 2009),

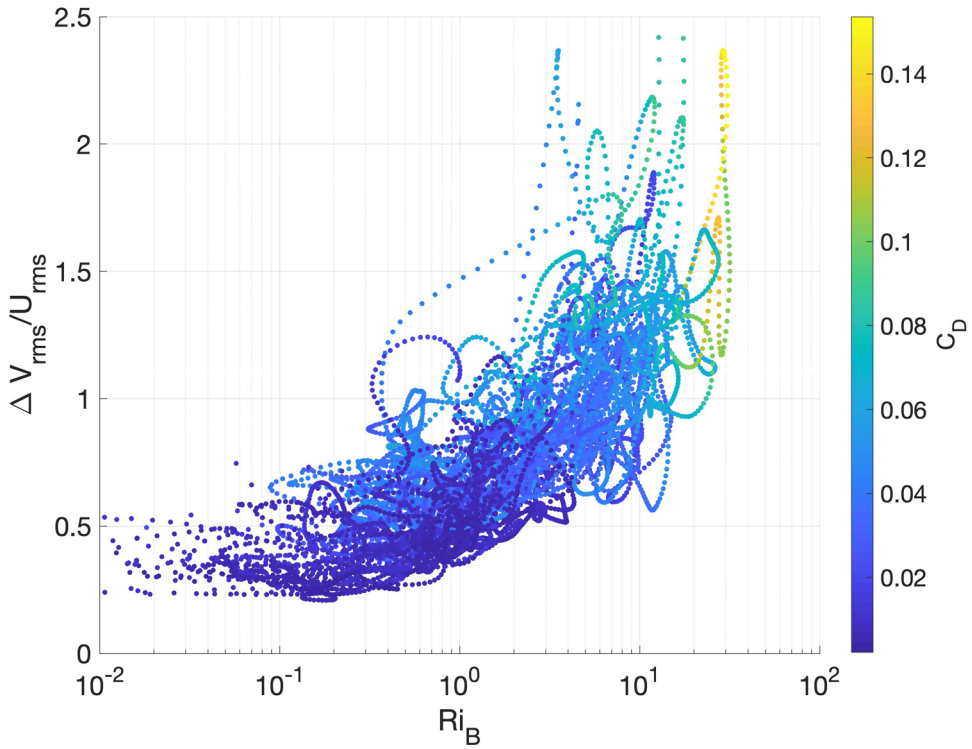

Fig. 9 Scaled secondary flow strength at Punta Prieta as a function of flow stability as observed between March 2013 and September 2015. The color scale indicates estimated values of C_D, which appear to increase with flow stability and secondary flow strength

although in that case, baroclinic pressure gradients were also important to the overall momentum balance.

Thus, it appears that the large values of C_D, i.e., values that are somewhat larger than what the $C_D(KB)$ model predicts, are due to the secondary flow associated with the headland. This secondary flow creates a shear-flow dispersion mechanism (Fischer et al. 1979) that retards the alongshore flow, as in the surf-zone flow model of Svendsen and Putrevu (1994). As argued by Kalkwijk and Booij (1986), the extra drag due to the secondary flow is inversely proportional to the rate of vertical mixing of momentum. Thus, as stratification increases, secondary flows might get stronger, and so total water column drag would increase, as seen in our data.

Summary and Conclusions

Exploiting a 3-year data set during which time kelp biomass varied substantially, we were able to estimate the dependence of the effective drag coefficient on kelp biomass, albeit as approximated from satellite imagery. The basis for this determination is a simplified 1D momentum balance that can be expressed using a single non-dimensional number P (Eq. (9)) that determines R, the ratio of the RMS depth-averaged value to its value in the absence of drag. Strikingly, we found that the effective drag coefficient for kelp was nearly independent of kelp biomass for values larger than about 0.1 kg/m^2 and reached a limiting value of ≈ 0.04, roughly a factor of 10 larger than the typical inner shelf bottom drag coefficients, and somewhat smaller than what has been inferred in the past (e.g., Jackson and Winant 1983). However, at times, C_D could be much larger than 0.04, behavior that we argue reflect the effects of secondary flows in the presence of stratification.

The large degree of variability in C_D as a function of kelp biomass that is apparent in our data points to the challenges inherent to knowing how much kelp, as measured by biomass/m^2, fronds/m^2, or by the thickness of the canopy layer, is present. Nonetheless, it is clear that more direct measurements of drag, ones that use measured pressure gradients (Lentz et al. 2017; Arzeno et al. 2018; Monismith et al. 2019), would be valuable, along with local in-water measurements of kelp abundance that could better ground-truth satellite data. Lastly, to be useful, any improved model of kelp drag should also properly account for waves (Gaylord et al. 2008; Rosman et al. 2013), a task that is made even more difficult due to motion of the kelp in the presence of surface waves.

Acknowledgements We are grateful to the fishers and staff of the cooperative Buzos y Pescadores without whom the data upon which this paper is based would never have been acquired, as well as our colleagues, Fio Micheli, Charlie Boch, Arturo Hernandez, Leonardo Vazquez-Vera, Geno Pawlak, and Jim Leichter.

Funding The work we describe here was supported by NSF grants OCE 1736830, OCE-1736957, OCE 1737090, and OCE 2022927, and by an equipment grant from the Kuwait Foundation for the Advancement of Sciences.

References

Alnajjar, M.W. 2019. Nearshore processes of a coastal island: physical dynamics and ecological implications. PhD thesis, Stanford University.

Arzeno, I.B., A. Collignon, M. Merrifield, S.N. Giddings, and G. Pawlak. 2018. An alongshore momentum budget over a fringing tropical fore-reef. *Journal of Geophysical Research (oceans)* 123: 7839–7855.

Bell, T.W., J.G. Allen, K.C. Cavanaugh and D.A. Siegel. 2020. Three decades of variability in California's giant kelp forests from the Landsat satellites. *Remote Sensing of Environment* 238 (1). https://doi.org/10.1016/j.rse.2018.06.039.

Boch, C.A., S. Litvin, F. Micheli, G. De Leo, E. Aalto, C. Lovera, B.C. Woodson, S. Monismith, and J.P. Barry. 2017. Effects of current and future coastal upwelling conditions on the fertilization success of the red abalone (Haliotis rufescens). *ICES Journal of Marine Science* 74 (4): 1125–1134.

Boch, C.A., F. Micheli, M. Alnajjar, S.G. Monismith, J.M. Beers, J.C. Bonilla, A.M. Espinoza, L. Vazquez, and C.B. Woodson. 2018. Local oceanographic variability influences the performance of juvenile abalone under climate change. *Scientific Reports* 8:5501. https://doi.org/10.1038/s41598-018-23746-z.

Cavole, L.M., A.M. Demko, R.E. Diner, A. Giddings, I. Koester, C.M.L.S. Pagniello, M.-L. Paulsen, A. Ramirez-Valdez, S.M. Schwenck, N.K. Yen, M.E. Zill, and P.J.S. Franks. 2016. Biological impacts of the 2013–2015 warm-water anomaly in the Northeast Pacific: Winners, losers, and the future. *Oceanography* 29: 273–285.

Di Lorenzo, E., and N. Mantua. 2016. Multi-year persistence of the 2014/15 North Pacific marine heat wave. *Nature Climate Change*. https://doi.org/10.1038/nclimate3082.

Fischer, H.B., E.J. List, R.C.Y. Koh, J. Imberger, and N.H. Brooks. 1979. *Mixing in inland and coastal waters*. Academic Press.

Gaylord, B., M.W. Denny, and M.A.R. Koehl. 2003. Modulation of wave forces on kelp canopies by alongshore currents. *Limnology and Oceanography* 48: 860–871.

Gaylord, B., J.H. Rosman, D.C. Reed, J.R. Koseff, J. Fram, and J., S. MacIntyre, S. K. Arkema, C. McDonald, M.A. Brzezinski, J.L. Largier, S.G. Monismith, P.T. Raimondi, and B. Mardian,. 2007. Spatial patterns of flow and their modification within and around a giant kelp forest. *Limnology and Oceanography* 52: 1838–1852.

Gaylord, B., M.W. Denny, and M.A.R. Koehl. 2008. Flow forces on seaweeds: Field evidence for roles of wave impingement and organism inertia. *Biological Bulletin* 215: 295–308.

Gaylord, B., K.J. Nickols, and L. Jurgens. 2012. Roles of transport and mixing processes in kelp forest ecology. *Journal of Experimental Biology* 215: 997–1007.

Godin, G. 1972. *The analysis of tides*. University of Toronto Press.

Grant, W.D., and O.S. Madsen. 1979. Combined wave and current interaction with a rough bottom. *Journal of Geophysical Research (oceans)* 84: 1797–1808.

Jackson, G.A., and C.D. Winant. 1983. Effect of a kelp forest on coastal currents. *Continental Shelf Research* 2: 75–80.

Kalkwijk, J.P.T., and R. Booij. 1986. Adaptation of secondary flow in nearly horizontal flow. *Journal of Hydraulic Research* 24: 19–37.

Lentz, S.J., K.A. Davis, J.H. Churchill, and T.M. DeCarlo. 2017. Coral reef drag coefficients–water depth dependence. *Journal of Physical Oceanography* 47 (5): 1061–1075.

Lentz, S.J., J.H. Churchill, and K.A. Davis. 2018. Coral reef drag coefficients-surface gravity wave enhancement. *Journal of Physical Oceanography* 48 (7): 1555–1566. https://doi.org/10.1175/JPO-D-17-0231.1.

Monismith, S.G., H. Hirsh, N. Batista, H. Francis, G. Egan, and R.B. Dunbar. 2019. Flow and drag in a seagrass bed. *Journal of Geophysical Research (oceans)*. https://doi.org/10.1029/2018JC0148622019.

Monismith, S.G., M.W. Alnajjar, C.B. Woodson, C.A. Boch, A. Hernandez, L. Vazquez-Vera, T.W. Bell, and F. Micheli. (unpublished). Influence of kelp forest state on the nearshore currents around an island. https://doi.org/10.25740/ng474qg6723.

Mullarney, J.C., and C.A. Pilditch. 2017. The differential response of kelp to swell and infragravity wave motion. *Limnology and Oceanography* 62: 2524–2537.

Nepf, H.M. 2012. Flow and transport in regions with aquatic vegetation. *Annual Reviews of Fluid Mechanics* 44: 123–142.

Nidzieko, N.J., S.G. Monismith, and J.L. Hench. 2009. Lateral circulation in well-mixed and stratified estuarine flows with curvature. *Journal of Physical Oceanography* 39 (4): 834–851.

Prandle, D., and M. RahmanM. 1980. Tidal response in estuaries. *Journal of Physical Oceanography* 10 (10): 1552–1573.

Reidenbach, M.A., S.G. Monismith, J.R. Koseff, G. Yahel, and A. Genin. 2006. Boundary layer turbulence and flow structure over a fringing coral reef. *Limnology and Oceanography* 51 (5): 1956–1968.

Rogers, J.S., S.A. Maticka, V. Chirayath, C.B. Woodson, J.J. Alonso, and S.G. Monismith. 2018. Connecting flow over complex terrain to hydrodynamic roughness on a coral reef. *Journal of Physical Oceanography* 48 (7): 1567–1587.

Rosman, J.H., J.R. Koseff, S.G. Monismith, and J. Grover. 2007. A field investigation into the effects of a kelp forest (Macrocystis pyrifera) on coastal hydrodynamics and transport. *Journal of Geophysical Research* (*Oceans*), 112. https://doi.org/10.1029/2005JC003430.

Rosman, J.H., S.G. Monismith, M.A. Denny, and J.R. Koseff. 2010. Currents and turbulence within a kelp forest (Macrocystis pyrifera): Insights from a dynamically scaled laboratory model. *Limnology and Oceanography* 55: 1145–1158.

Rosman, J.H., M.W. Denny, R.B. Zeller, S.G. Monismith, and J.R. Koseff. 2013. Interaction of waves and currents with kelp forests (*Macrocystis pyrifera*): Insights from a dynamically scaled laboratory model. *Limnology and Oceanography*. https://doi.org/10.4319/lo.2013.58.3.0790.

Rosman, J.H., and J.L. Hench. 2011. A framework for understanding drag parameterizations for coral reefs. *Journal of Geophysical Research (oceans)* 116: C08025. https://doi.org/10.1029/2010JC006892.

Stacey, M.T., S.G. Monismith, and J.R. Burau. 1999. Observations of turbulence in a partially stratified estuary. *Journal of Physical Oceanography* 29: 1950–1970.

Street, R.L, G.Z. Watters, and J.K. Vennard. 1996. *Elementary fluid mechanics 7ed*. J. Wiley.

Svendsen, I.A., and U. Putrevu. 1994. Nearshore mixing and dispersion. *Proceedings of the Royal Society of London Series A* A445: 561–576.

Utter, B.D., and M.W. Denny. 1996. Wave-induced forces on the giant kelp *Macrocystis pyrifera* (AGARDH): Field test of a computational model. *Journal of Experimental Biology* 199: 2645–2654.

Valle-Levinson, A., M.A. Daly, B. Juarez, M. Fagundes, C.B. Woodson, and S.G. Monismith. 2022. Influence of kelp forests on flow around headlands. *Science of the Total Environment* 825: 153952. https://doi.org/10.1016/j.scitotenv.2022.153952.

Woodson, C.B., F. Micheli, C. Boch, M. Al-Najjar, A. Espinoza, A. Hernandez, L. Vázquez-Vera, A. Saenz-Arroyo, S.G. Monismith, and J. Torre. 2018. Harnessing marine microclimates for climate change adaptation and marine conservation. *Conservation Letters*. https://doi.org/10.1111/conl.12609.